Journal of Hydrology 578 (2019) 124019

Contents lists available at ScienceDirect

Journal of Hydrology

journal homepage: www.elsevier.com/locate/jhydrol

Research papers

Preferential water flow: Influence of alfalfa (*Medicago sativa* L.) decayed root channels on soil water infiltration

Lei Guo[a,1], Yu Liu[a,b,1], Gao-Lin Wu[a,b,d,*], Ze Huang[a], Zeng Cui[a,b], Zhen Cheng[a], Rui-Qi Zhang[a], Fu-Ping Tian[c], Honghua He[a,b]

[a] State Key Laboratory of Soil Erosion and Dryland Farming on the Loess Plateau/College of Natural Resources and Environment, Northwest A&F University, Yangling, Shaanxi, China
[b] Institute of Soil and Water Conservation, Chinese Academy of Sciences and Ministry of Water Resource, Yangling, Shaanxi 712100, China
[c] Lanzhou Institute of Husbandry and Pharmaceutical Sciences of Chinese Academy of Agricultural Sciences, Lanzhou, Gansu 730050 China
[d] CAS Center for Excellence in Quaternary Science and Global Change, Xi'an 710061, China

ARTICLE INFO

This manuscript was handled by Marco Borga, Editor-in-Chief, with the assistance of Daniele Penna, Associate Editor

Keywords:
Soil water infiltration rate
Root channels
Double-ring infiltrometer
Preferential flow
Soil water supply

ABSTRACT

Soil water infiltration is an important part of the land surface hydrological cycle, and plays an important role in the hydrological response of the soil, such as soil erosion. High infiltration rates favor an increase in the soil water storage capacity that allows maintaining vegetation restoration in arid and semi-arid regions. Alfalfa (*Medicago sativa* L.) is a quality perennial legume grassland, which is widely planted in semi-arid areas. In this study, the effects of the root channels formed by the decay of alfalfa on preferential flow were evaluated as a driving force to improve soil water infiltration and soil water supply. A double-ring infiltrometer (30-cm inner diameter and 60-cm outer diameter) was used to measure the infiltration process with the falling head method. Methylene blue was used to visualize the pathways followed by the infiltrated water. The results showed that the initial infiltration rate in the alfalfa grassland increased by 27.7%, compared with the control bare land, and the total cumulative infiltration was 1.13 times higher. The steady infiltration rate of the grassland increased by 31.8% compared to the bare land. The root channel diameters were measured with a Vernier caliper, and the average root channel area (RCA) was calculated through the average root channel diameter (ARCD). The values of ARCD and RCA were significantly and positively correlated with the infiltration rates, being the coefficients of determination 0.815 and 0.789, respectively. Our results indicated that root channels formed by the decayed roots of alfalfa played an important role in increasing soil water infiltration and soil water supply under semi-arid conditions. Our research improves the understanding of the hydrological cycle processes at the plant-soil interface in semi-arid areas.

1. Introduction

Land surface water resources shortage and their effective utilization are among the most serious problems in farmlands, particularly in arid and semi-arid regions (Yin et al., 2018). Soil water is one of the most important limiting factors that influences vegetation growth and distribution patterns in arid and semi-arid areas (Wang et al., 2007, 2008; Wu et al., 2017). Under these conditions, any decrease in soil water could aggravate soil water shortage in both the top and deep soil layers, and even favor the formation of the dry soil layer, further endangering the sustainability of vegetation restoration (Jia et al., 2017, 2019). Furthermore, soil water availability for plants is a clear limiting factor that affects vegetation survival, growth and restoration in arid and semi-arid areas, because rainfall is the only source that can replenish soil water (Wang et al., 2007). The study of water infiltration is therefore crucial for its ecological significance.

Soil matrix and preferential flow are the two main forms of water infiltration into the soil (Jarvis et al., 2012). Matrix flow refers to the relatively slow movement of water and solutes through the soil, while passing through all pore spaces (Allaire et al., 2009). Preferential flow is defined as the physical movement of water and solutes along certain pathways, while bypassing a fraction of the pore matrix (Hendrickx and Flury, 2001). Preferential flow may accelerate or delay the movement of water and solutes depending upon the position of the water and solutes compared to the position of the preferential flow paths (Allaire et al., 2009). However, preferential flow is randomly distributed in the

* Corresponding author at: State Key Laboratory of Soil Erosion and Dryland Farming on the Loess Plateau, Northwest A&F University, Yangling, Shaanxi, China.
E-mail address: wugaolin@nwsuaf.edu.cn (G.-L. Wu).
[1] These authors contributed equally to this work and are co-first authors.

https://doi.org/10.1016/j.jhydrol.2019.124019
Received 19 April 2019; Received in revised form 17 July 2019; Accepted 3 August 2019
Available online 06 August 2019
0022-1694/

soil, spatially and temporally, and thus is essentially unpredictable (Hendrickx and Flury, 2001; Zhang et al., 2015, 2017). Preferential flow occurs in most soils and is caused from a series of factors such as macropore flow, non-homogeneous infiltration, lateral flow, and wetting front instabilities (Allaire et al., 2009; Bundt et al., 2001).

To visualize preferential water flow pathways in soils, dye traces are often used (Flury and Flühler, 1994; Ghodrati and Jury, 1990; Flury and Wai, 2003). Brilliant Blue FCF (C. l. Food Blue 2) has often been used for its lower adsorption and higher mobility (Flury and Flühler, 1994), although ions and isotopes have been also employed to distinguish preferential and matrix flow paths (e.g., Bogner et al., 2008; Backnäs et al., 2012; Ma et al., 2017; Jaromir and Tomas, 2018). Zhang et al. (2015) used Brilliant Blue solution, at a concentration of $5\,g\,L^{-1}$, to identify preferential flow pathways through dye coverage; and the maximum depth of infiltration could also be determined. Weiler and Flühler (2004), and Cey and Rudolph (2009) suggested that the type of macropore flow and the interaction between macropore flow and matrix flow can be understood after mapping dye concentration by using classification techniques or image analysis software.

Numerous methods for measuring infiltration have been developed and applied, such as the single ring infiltrometer (Reynolds and Elrick, 1990; Wu et al., 1999), the double-ring infiltrometer (Bouwer, 1986), the disc permeameter (Perroux and White, 1988; Ankeny et al., 1988; López-Vicente and Álvarez, 2018), the rainfall simulator (Peterson and Bubenzer, 1986; Ogden et al., 1997; Mao et al., 2011), the point source method (Mao et al., 2016), the run off-on-out method (Liu et al., 2010), and the Guelph permeameter (López-Vicente and Navas, 2009; Rodrigo Comino et al., 2016, 2017). The ring infiltrometer is the most commonly used method for measuring soil infiltration rates (Walsh and McDonnell, 2012). According to Zhang et al. (2016), and using the single-ring infiltrometer, preferential flow encourages higher initial infiltration rates. Wu et al. (1997) compared the constant and falling head methods with numerical modelling, obtaining similar soil infiltration rates in fine textured soils, although soil infiltration rates decreased more than 30% with the decrease of the water head in coarse soils. The double-ring infiltrometer is frequently used to measure infiltration because this device is relatively inexpensive, simple and easy to operate; nevertheless, errors in the experimental results are not infrequent and are well documented. Zhang et al. (2016), for example, described the effect of preferential flow on the measurement accuracy of infiltration rates caused by the disturbance of soil when infiltrometer is inserted into the ground. Zhang et al. (2017), in order to avoid preferential flow in measuring infiltration in forest soil, added a layer of fine sand to the inner and outer rings and found that the measured infiltration reflected the transient process of soil matrix infiltration and the results were consistent with the values generated by accepted infiltration models. The disc permeameter, unlike the infiltrometer, forces water to penetrate into the soil under negative water potentials previously determined by the operator; therefore, it can only measure the hydraulic characteristics of unsaturated soil (Logsdon and Jaynes, 1993; Angulo-Jaramillo et al., 2000). Hence, this method cannot measure soil infiltration on soil surface under positive pressure conditions. Besides, the soil hydraulic conductivity measurement under ponded infiltration conditions is not ensured by using this method (Reynolds and Zebchuk, 1996). Rainfall simulation is often used to measure infiltration rates (Smets et al., 2011; Iserloh et al., 2013), and study soil erosion and other soil hydrological processes (Lassu et al., 2015; Keesstra et al., 2016). It is known that the different methods and techniques provide distinct soil water infiltrations rates under the same conditions. Cerda (1997) reported that the infiltration rates estimated by the ring infiltrometer were 8–8.5 times higher than those obtained by rainfall simulator based on 40 groups of field measurements. Furthermore, Mao et al. (2011) revealed that the initial infiltration rate measured by the rainfall simulator was not accurate under heavy rainfall conditions.

A point source method was developed by Su (2007) for measuring in situ infiltration rates, obtaining lower rates than those rates measured with the linear source method; although the point source method had higher accuracy and lower relative error. The use of this method formed a circular or near-circular wet area at the soil surface, which increased gradually over time to reach a final wet area (Mao et al., 2016). Channels formed by plant roots are common preferential soil flow pathways both for water and solutes (Bogner et al., 2010; Germann et al., 2012; Zhang et al., 2017). The alfalfa's root system is characterized by a large-diameter, long, almost-straight taproot. When alfalfa dies and decays, it provides a temporary channel for macropore flow (Mitchell et al., 1995). Old root channels that have been opened at the soil surface (Wang and Strong, 1996), and root channels created by decayed roots in the vertical direction (Mitchell, 1995), are both regarded as macropores. Water infiltration into soil through root channels is an important mechanism of soil infiltration and plays an important role in predicting runoff generation and groundwater recharge (Weiler and Naef, 2003). Macropores formed by plant roots are crucial for the soil water downward movement, especially in arid and semi-arid areas. Wu et al. (2017) found that the initial infiltration rate and the average infiltration rate during the first 15 min increased as the diameter of root channels increased. Mitchell (1995), and Benegas et al. (2014) concluded that tree roots, including both living and decaying roots, have positive effects on soil infiltration by increasing macroporosity and soil aggregation. More than sixty years ago, Barley (1954) also illustrated that plant roots increased the soil infiltration rate.

Although previous studies have addressed the effects of root systems on soil water infiltration, the influence of root channels formed by decayed roots is scarcely studied. This theme, especially in arid and semi-arid regions, where soil-water availability for plant is essential, deserves to be studied in depth. The objectives of this study were: (1) to determine the decayed roots in response to preferential flow paths, and (2) to further explore the relationships between the properties of the channels formed by the decayed roots, and the soil water infiltration process.

2. Materials and methods

2.1. Study sites

This study was conducted at the Key Field Observation Station of Ecological Environment of the Ministry of Agriculture on the Loess Plateau, which is located in Gongjiawan district, Lanzhou city, in Gansu Province, China (36°01′N, 103°45′W), as shown in Fig. 1. This area belongs to the arid hilly and gully regions on the Loess Plateau (altitude ranging from 1698 to 1823 m a.s.l.), which is characterized by a semi-arid and continental climate. Between 2001 and 2013, the mean annual precipitation and evaporation were 383 and 1450 mm, respectively. Rainfall events were unevenly distributed, and mainly concentrated in July, August and September. The average annual temperature was 7.4 °C, and the highest and lowest recorded temperature were 19.8 °C in July and −7.2 °C in January. The mean annual sunshine duration was about 2651 h, and the frost-free period ranged between 135 and 167 days.

The soil is mainly loessial, and the loess layer thickness is approximately 150 m. Within the fine soil fraction (< 2 mm of diameter), the mean content of sand, silt and clay is 25.5%, 66.1% and 8.4%, respectively (determined by laser diffraction using a Mastersizer 2000, Malvern Instruments), according to the USDA texture classification. The soil moisture at field capacity, by mass, ranges between 19.3% and 22.6% (Huang et al., 2017), and the mean soil organic matter content is ca. $27.2\,g\,kg^{-1}$ for the 0–30 cm depth layer.

2.2. Experimental plots and infiltration measurements

The experimental site was a cultivated alfalfa (*Medicago sativa* L.) field, where plants remained dead for 3–5 years. Other grass species like

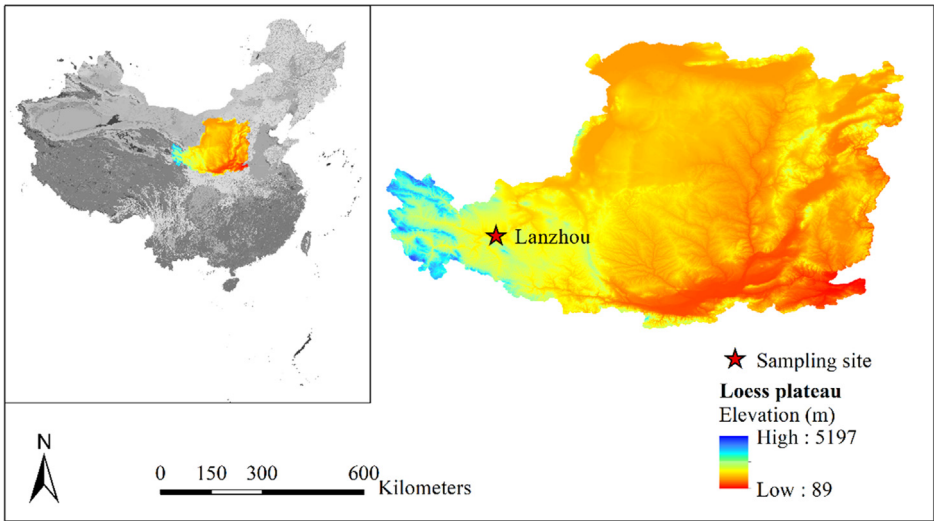

Fig. 1. Location of the experimental site on the Loess Plateau, Central China.

Leymus secalinus, Artemisia sacrorum, Artemisia annua and Artemisia incisa, etc. grew in the alfalfa field after the death of *Medicago sativa*. Three alfalfa field research areas, each area of 10 × 10 m, were established in the grassland. Seeds were planted with a row spacing of 50 cm, and at a sowing rate of 0.07 kg m^{-2}. In the process of planting, the sowing rate was slightly higher than usual in order to improve the emergence rate, owing to the barren soil conditions.

Alfalfa grass growth depended on rainfall; there were no additional fertilizations, human interventions or animal disturbances, and these conditions were similar in all plots during all the experimental treatments. These treatments included alfalfa grassland and bare land; in addition, the alfalfa grassland was treated with or without a fine sand layer. The purpose of the fine sand layer was to avoid the occurrence of preferential flow. Six experimental plots were randomly selected at each experimental treatment and set as six replicates. Infiltration measurements were carried out in all the treatments: alfalfa, with (6 measurements) and without (6 measurements) fine sand, and bare soil (6 measurements). The double-ring infiltrometer was used to measure water infiltration (Fig. 2).

After selecting a level site, the litter layer was carefully removed so that the soil surface was exposed. Then, the rings (30-cm diameter inner ring, 60-cm diameter outer ring, both 20-cm in height) were placed concentrically on the soil surface and were gently inserted 10 cm vertically into the soil, in order to reduce crack formation. Some soil was then placed outside of the inner and outer rings to avoid water outflow. The inner and outer rings were filled with water, with and without methylene blue, respectively, until the water depth reached 5 cm at the same time in both rings. When methylene blue was dissolved in water, the solution appeared bright blue. The falling head method was used to measure water infiltration. The time required to infiltrate water, up to the water level dropped 1 cm in the inner ring, was recorded with a stopwatch until the infiltration time did not change for three consecutive measurements, and this rate was assumed as the steady-state infiltration. During the infiltration tests, water was refilled into the rings whenever the water level dropped to 1 cm depth, and the water levels in the inner and outer rings were consistent. To calculate the initial infiltration rate, only the first three minutes of the infiltration process were taken into consideration. In fact, the initial infiltration rate was an average rate because we took into account the total three minutes of infiltrated water. The average of the last three fairly constant infiltration rates was considered as the steady-state infiltration rate. These rates were calculated following the equation of Zhang et al. (2017):

$$i = \Delta I/\Delta t \times 600 \quad (1)$$

where i is the infiltration rate (mm h^{-1}), ΔI is the cumulative infiltration in the inner ring (cm) during Δt time of infiltration (min), and 600 is a unit conversion factor.

To evaluate the role played by the root channels in the preferential flow, other double-ring infiltrometer was applied to measure the infiltration process in the alfalfa grassland with the fine sand layer (6 measurements). According to the methods of Zhang et al. (2017), a

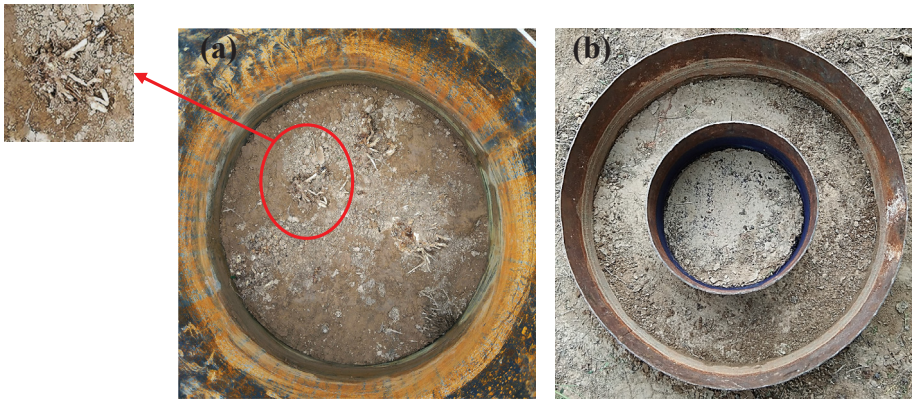

Fig. 2. Pictures of the infiltrometer rings used to measure the soil water infiltration in two experimental treatments.

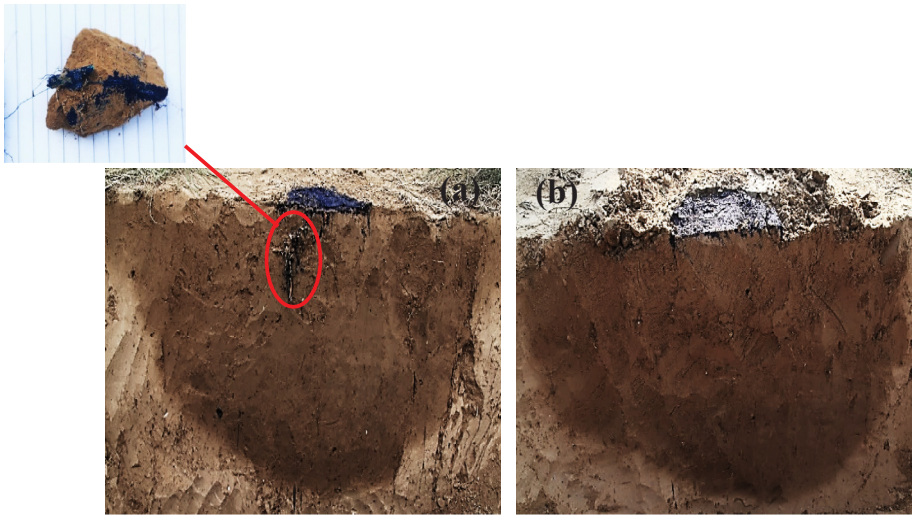

Fig. 3. Pictures of the vertical soil profiles below the inner infiltrometer rings 24 h after ending the infiltration tests, in two experimental treatments.

layer of nylon cloth was placed on the soil surface inside the inner ring and between the inner and outer rings, and then a layer of fine sand, of 1–3 cm thick, was evenly placed on the nylon cloth, in order to avoid the occurrence of preferential flow and to ensure that water infiltrates the soil surface only through the soil matrix. To reduce the scouring of the fine sand layers while the rings were filled with water, paperboards were placed on the sand surface. In the infiltration tests with sand, measurements were carried out following the same method mentioned above.

2.3. Soil sampling and analysis

Twenty-four hours after the end of the infiltration tests, vertical soil profiles were excavated passing through the center of the inner ring. The vertical soil profiles are shown in Fig. 3 for alfalfa and bare land treatments. The width and depth of the wetted soil area were then measured with a steel ruler, having the smallest division of 1 mm. The wetted vertical profiles were recorded with a camera, in order to distinguish the spots stained by the tracer dye. Afterwards, soil samples were collected throughout the entire soil profile (0–100 cm), at 10-cm intervals, on the other side of the excavation trench. Three replicates were collected at each soil layer, and the soil water content by mass (SWC, % weight) and soil bulk density (BD, g cm^{-3}) were determined. The SWC was measured by taking the proportion of the loss of mass, after oven-drying at 105 °C, to the constant mass of dry soil. The BD was measured using a stainless-steel cutting ring sampler of 5-cm diameter and height (393 cm^3) to collect the samples. The soil total porosity (TP, %) was calculated using the following equation:

$$TP = (1 - BD/ds) \times 100 \quad (2)$$

where ds is the soil particle density (g cm^{-3}), which was assumed to be 2.65 g cm^{-3} (Huang et al., 2017). The mean and standard error values of the soil physical properties are shown in Table 1.

2.4. Root channels measurement

The diameter of the root channels, i.e. the diameter of the stubbles on the ground, were only measured in the inner ring of the twelve alfalfa experimental plots by using a Vernier caliper (having a Vernier constant of 0.10 mm). The average value of the stubble diameters was regarded as the average diameter of root channels, which we assumed that have influenced the preferential water flow (Wu et al., 2017). Meanwhile, to estimate the area of the root channels, the total number of root channels was counted in the inner ring at each experimental site. According to the methods of Wu et al. (2017), the following formulas were used to calculate the average root channels diameter (ARCD, cm), and the root channel area (RCA, cm^2).

$$ARCD = \sum_{i=1}^{n} d/n \quad (n = 1, 2, 3...) \quad (3)$$

$$RCA = n \cdot \pi \cdot ARCD^2/4 \quad (n = 1, 2, 3...) \quad (4)$$

where di is the diameter of the root channel (cm), n is the number of root channels.

Table 1
Mean ± standard error values of the soil physical properties (SWC: soil water content by mass; BD: soil bulk density; TP: soil total porosity) for the entire soil profile (0–100 cm).

Treatments	Soil depth (cm)	SWC (%)	BD (g cm^{-3})	TP (%)
Grassland	0–10	2.67 ± 0.02a	1.31 ± 0.03a	50.10 ± 1.24a
	10–20	3.87 ± 0.86a	1.33 ± 0.58a	49.98 ± 1.94a
	20–30	3.69 ± 0.53a	1.48 ± 0.05a	44.15 ± 2.04a
	30–40	4.19 ± 1.26a	1.38 ± 0.07a	47.75 ± 2.69a
	40–50	4.07 ± 0.92a	1.23 ± 0.03b	53.42 ± 1.28a
	50–60	3.56 ± 0.52a	1.24 ± 0.07b	53.07 ± 2.79a
	60–70	3.58 ± 0.63a	1.23 ± 0.06a	53.60 ± 2.42a
	70–80	3.58 ± 0.02b	1.22 ± 0.01b	53.86 ± 0.41a
	80–90	3.39 ± 0.24a	1.24 ± 0.03b	53.08 ± 1.26a
	90–100	3.14 ± 0.11a	1.24 ± 0.01b	53.07 ± 0.57a
Bare land	0–10	2.71 ± 0.03a	1.28 ± 0.07a	51.57 ± 2.51a
	10–20	3.91 ± 0.87a	1.36 ± 0.09a	48.49 ± 3.28a
	20–30	3.72 ± 0.58a	1.49 ± 0.04a	43.78 ± 1.45a
	30–40	4.26 ± 1.31a	1.48 ± 0.02a	43.94 ± 0.65a
	40–50	4.14 ± 0.12a	1.45 ± 0.06a	45.22 ± 2.23b
	50–60	3.67 ± 0.58a	1.44 ± 0.05a	45.49 ± 1.81b
	60–70	3.69 ± 0.71a	1.32 ± 0.03a	50.04 ± 1.21a
	70–80	3.70 ± 0.14a	1.36 ± 0.04a	48.71 ± 1.63b
	80–90	3.48 ± 0.33a	1.35 ± 0.03a	49.06 ± 2.16b
	90–100	3.21 ± 0.18a	1.33 ± 0.02a	49.81 ± 1.84a

Note: Real density was assumed to be 2.65 g cm^{-3}. For each soil depth but different treatment, the values followed by a different letter are significantly different at 0.05 level.

2.5. Statistical analysis

The statistical analyses were conducted using SPSS software (ver. 22.0). One-way analysis of variance (ANOVA) was used to determine if

the differences in the soil properties between each experimental treatment were statistically significant with a p-value of 0.05. Regression analysis was used to determine relationships between the maximum infiltration depth, the diameter of root channels, the area of root channels, the number of root channels and the steady-state infiltration rate. The coefficient of determination (R^2) was used to evaluate the performance of the applied regression equations.

3. Results

3.1. Soil properties in different treatments

The differences in the soil physical properties of the different treatments are shown in Table 1. Overall, the SWC and BD were lower in the *Medicago sativa* grassland than in the bare land, whereas opposite differences were found for the TP. A significant difference between *Medicago sativa* grassland and bare soil was found for SWC for the 70–80 cm soil depth, although the differences were not significant for the other soil layers. The BD was significantly lower in *Medicago sativa* grassland than in bare land for all the soil depths greater than 40–50 cm. The TP was significantly higher in the *Medicago sativa* grassland than in the bare land for the soil depths of 40–50, 50–60, 70–80, and 80–90 cm.

3.2. Soil water infiltration in the decayed root channels

The infiltration rates and cumulative infiltration curves of all the experimental treatments are shown in Fig. 4. The initial infiltration rate was high, as usual in this study, in all treatments; it decreased with time and finally reached a stable state. The different soil water infiltration rates in *Medicago sativa* were always higher than those rates found in the bare land (Fig. 4). Compared with the bare land, where the initial infiltration rate was 190.48 mm h^{-1}, the same rate in the *Medicago sativa* grassland was 27.70% greater, reaching up to 243.24 mm h^{-1} (Figs. 4a, 5). At the end of the experiment, the cumulative infiltration in the alfalfa fields was 1.13 times the value obtained in the bare land (Fig. 4b). In addition, our results revealed significant differences in the steady-state infiltration rate between the different experimental treatments (Fig. 5). The steady-state infiltration rate in the *Medicago sativa* grassland was higher than that observed in the bare land. In particular, the steady-state infiltration rate in the alfalfa grassland (73.32 mm h^{-1}) was 31.80% greater than the value estimated in the bare land (55.62 mm h^{-1}). Moreover, when the infiltration rate reached a steady-state value, there was a positive and strong correlation ($R^2 = 0.825$) between the steady-state infiltration rate and the maximum depth reached by the water along the soil profile (Fig. 6). This means that the higher depth the water penetrated into the soil, the higher steady-state infiltration rates were reached. The maximum depth reached by the infiltrated water was ca. 96 cm in the alfalfa grassland, and ca. 63 cm in the bare land plots (Fig. 3). We concluded that preferential flowpaths increased water penetration into the soil, owing to the decay of the alfalfa roots.

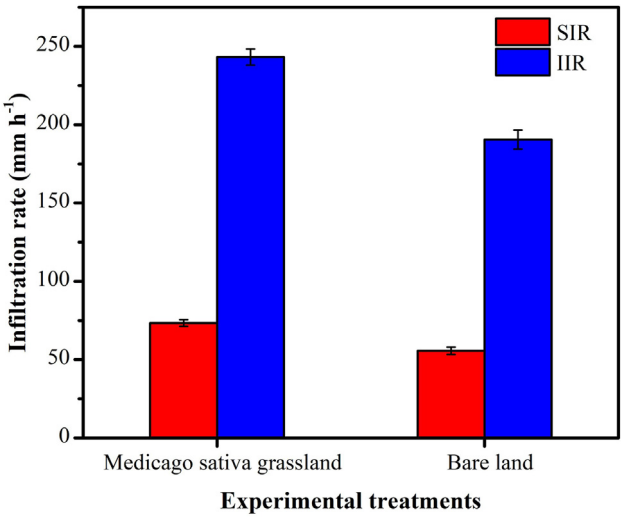

Fig. 5. Mean infiltration rates and their standard deviation in two different experimental treatments. Note: SIR is the steady-state infiltration rate; IIR is the initial infiltration rate (first initial 15 min for each test).

3.3. Relation between root channel properties and soil water infiltration

The correlation analyses showed that the average root channel diameter was positively correlated ($R^2 = 0.815$, $p < 0.01$) with the steady-state infiltration rate (Fig. 7b). Likewise, there was a significant relationship ($R^2 = 0.789$, $p < 0.01$) between the root channel area and the steady-state infiltration rate (Fig. 7c). In other words, the infiltration rate increased with the increase of the ARCD and RCA values. The number of root channels was also significantly and positively correlated ($R^2 = 0.797$, $p < 0.01$) with the steady-state infiltration rate (Fig. 7a).

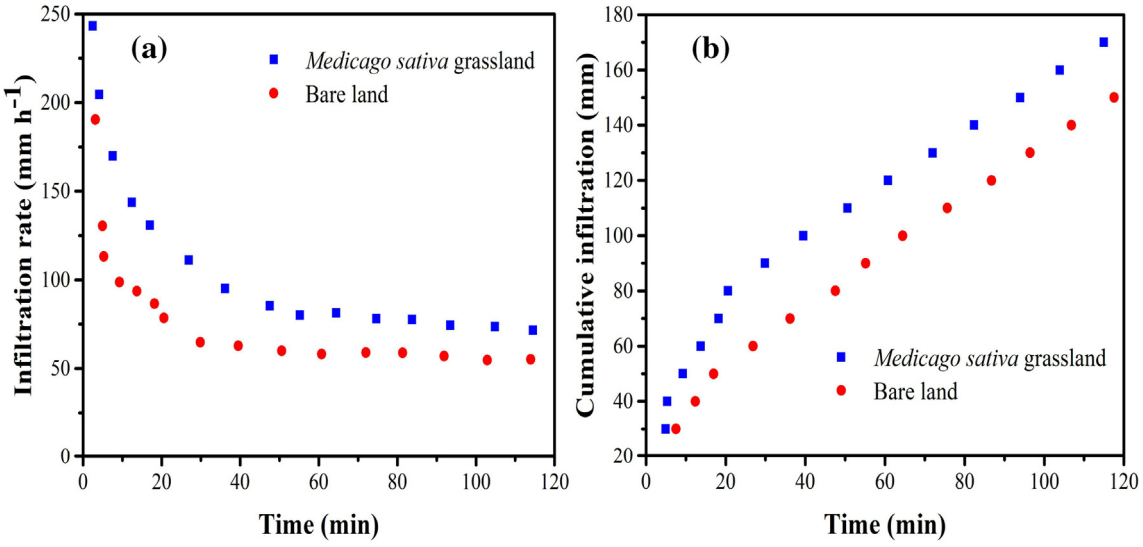

Fig. 4. Infiltration rate (a) and cumulative infiltration (b) curves for the experimental treatments.

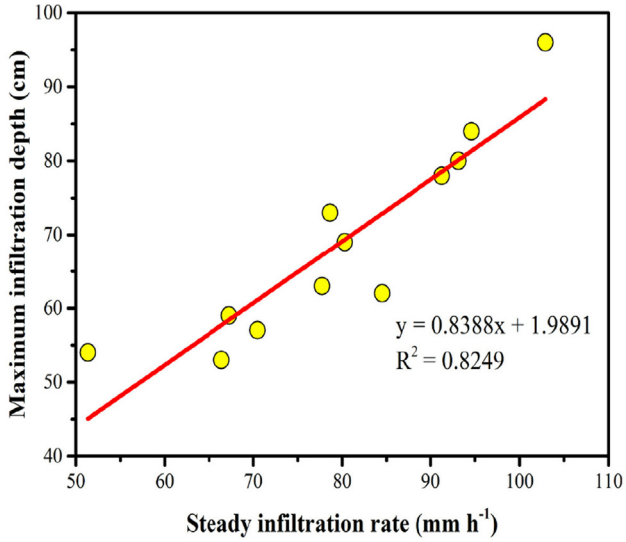

Fig. 6. Relationship between the steady-state infiltration rate and the soil water infiltration depth. Note: The maximum infiltration depth, indicated on the vertical axis, is the maximum depth the water reached along the soil profile after 24 h.

4. Discussion

Soil water infiltration is related to surface runoff, soil erosion, plant water storage and groundwater recharge (Jiang et al., 2018). In addition, water flow behavior is increasingly considered as the main factor of soil water distribution (Jiang et al., 2017). In our study, the steady-state infiltration rate of alfalfa was higher than that of the bare land. Consistent with the finding of Meek et al. (1990), the effect of alfalfa-root-induced macropores was mainly demonstrated by the increase of final infiltration rate when alfalfa roots decayed. Schematically, there are two main forms of water infiltration in the soil: matrix flow and preferential flow (Jarvis et al., 2012). Soil matrix flow, which is present in unsaturated conditions, is affected by capillary suction, and the process of infiltration is well matched with Philip's sorptivity concept (Zhang et al., 2017). Preferential flow, mainly due to gravitational potential, which is generally in the vertical direction (Germann et al., 2007), is caused by a number of factors such as macropore flow, non-homogeneous infiltration, lateral flow and wetting front instabilities (Allaire et al., 2009; Bundt et al., 2001) and, therefore, is difficult to describe with current theories, such as Richard's and Darcy-type equations (De Vries and Chow, 1978; Weiler, 2005).

Brilliant Blue dye is an important tool to prove the existence of preferential flow (Flury et al., 1994). Our study showed that most of the dye covered the top soil (Fig. 3) and this result was in agreement with the findings of Devitt and Smith (2002). Several studies showed that the dye coverage was lower in the subsoil than at the soil surface, because preferential flow was more frequent in the upper soil layers than in the deeper ones (Zhang et al., 2015). Furthermore, Mitchell et al. (1995) illustrated that the dyeing depth went below 55 cm along the decayed root channels, more likely because the roots influenced the physical properties of the soil, such as porosity and bulk density (Aubertin, 1971). The decayed root channels, tagged with blue dye inside (Fig. 3a), were a clear indication of pore space creation by the alfalfa roots. Dye was found around the roots, and the dye coverage decreased with the soil depth. When a root decayed, a clear porous soil remained, which was characterized by lower density and higher porosity, providing new space for water and air storage.

Our results were in agreement with those of Mitchell et al. (1995) and Barley (1954), who indicated that root channels, created by decayed roots, increased the infiltration rate. The existence of preferential flow resulted in the enhancement of soil infiltration capacity. After alfalfa died, the channels formed by the decayed roots were the main preferential flow that provided a temporary channel for macropore flow (Mitchell et al., 1995), as shown in Fig. 3a. Root channels would increase macropores network density and continuity, and channels formed by plant roots may be conducive to water transport and solute movement as preferential flow (Bogner et al., 2010; Germann et al., 2012). In general, and compared with living roots, it was much easier for decayed roots to form long and continuous preferential flow pathways that facilitated the downward movement of water (Mitchell et al., 1995). Additionally, we also found that the ARCD and RCA showed a positive correlation with the infiltration rates (Fig. 7b, c). This result agreed with the observations reported by Wu et al. (2017), who illustrated that the ARCD and RCA were positively correlated with the average infiltration rate calculated during the 0–15 min time interval and the initial infiltration rate. Lastly, it must be noted that the roots of legumes, such as alfalfa, are more effective creating stable macropores than those of gramineous plants, which contribute to increasing infiltration rates and benefit the higher proliferation and weight of leguminous roots (Wu et al., 2016).

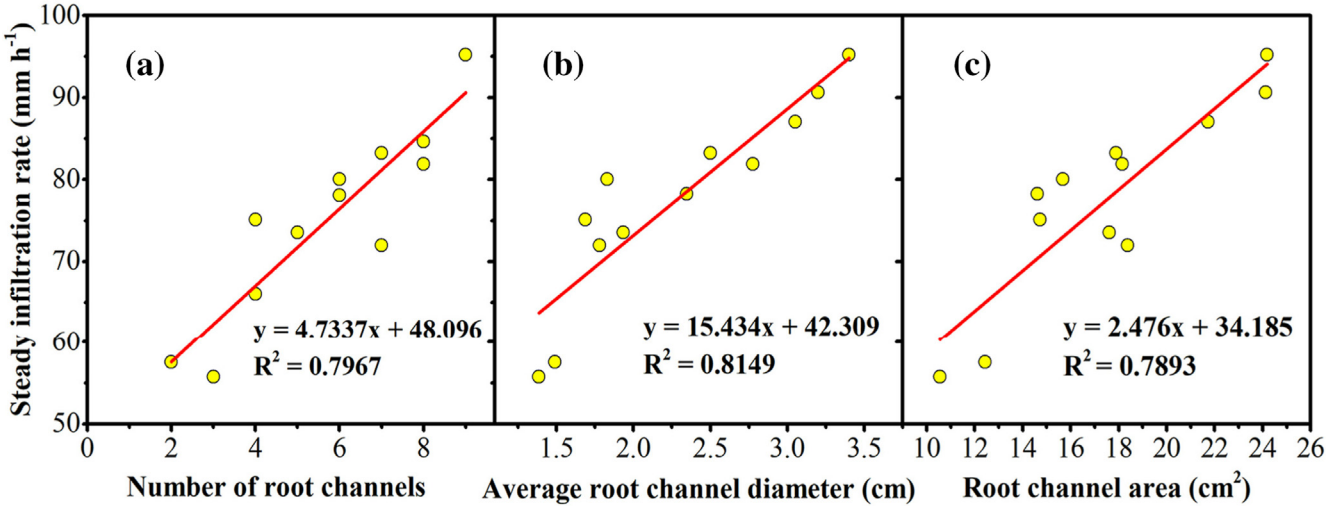

Fig. 7. Relationships between the number of root channels (a), the average root channel diameter (b) and the root channel area (c) vs. the steady-state infiltration rate.

5. Conclusions

This study demonstrated that the decayed root channels of alfalfa had significant effects on soil water infiltration in a loessial cultivated soil under semi-arid conditions. Compared to bare soil, the initial soil water infiltration rate in the *Medicago sativa* grassland increased by 27.70% and the cumulative infiltration was 1.13 times higher. Moreover, the steady infiltration rate in the grassland increased by 31.80%, compared with the bare land control plots. Our results indicated that root channels created by the alfalfa decayed roots played a significant role in increasing infiltration rate. The root diameter and area of the root sections, indicated previously with the terms ARCD and RCA, were significantly and positively correlated with the infiltration rate, being respectively 0.815 and 0.789 the coefficients of determination. Our results supported the conclusion that the decayed root channels of alfalfa significantly enhanced infiltration of water from soil surface toward deeper layers. Further research on this phenomenon could contribute to better understanding on the land surface water hydrological cycle process in arid areas.

Acknowledgements

We thank the editors and reviewers for their constructive comments and valuable suggestions on this work, and thank Dr. Manuel López-Vicente for improving the language of this manuscript. This research was funded by the National Natural Science Foundation of China (NSFC 41722107), the Light of West China Program of the Chinese Academy of Sciences (XAB2015A04, XAB2018B09), the Youth Talent Plan Foundation of the Northwest A&F University (2452018025), and the Agricultural Science and Technology Innovation Program of the Chinese Academy of Agricultural Sciences (CAAS-ASTIP-2016-LIHPS-08).

References

Allaire, S.E., Roulier, S., Cessna, A.J., 2009. Quantifying preferential flow in soils: a review of different techniques. J. Hydrol. 378, 179–204.
Angulo-Jaramillo, R., Vandervaere, J.P., Roulier, S., Thony, J.L., Gaudet, J.P., Vauclin, M., 2000. Field measurement of soil surface hydraulic properties by disc and ring infiltrometers: a review and recent developments. Soil Till. Res. 55, 1–29.
Ankeny, M.D., Kaspar, T.C., Horton, R., 1988. Design for an automated tension infiltrometer. Soil Sci. Soc. Am. J. 52, 893–896.
Aubertin, G.M., 1971. Nature and extent of macropores in forest soils and their influence on subsurface water movement. U.S.D.A. Forest Service Research Paper NE–192.
Backnäs, S., Laine-Kaulio, H., Kløve, B., 2012. Phosphorus forms and related soil chemistry in preferential flowpaths and the soil matrix of a forested podzolic till soil profile. Geoderma 189–190, 50–64.
Barley, K.P., 1954. Effects of root growth and decay on the permeability of a synthetic sandy loam. Soil Sci. 78, 205–210.
Benegas, L., Ilstedt, U., Roupsard, O., Jones, J., Malmer, A., 2014. Effects of trees on infiltrability and preferential flow in two contrasting agroecosystems in Central America. Agric. Ecosyst. Environ. 183, 185–196.
Bogner, C., Wolf, B., Schlather, M., Huwe, B., 2008. Analysing flow patterns from dye tracer experiments in a forest soil using extreme value statistics. Eur. J. Soil Sci. 59, 103–113.
Bogner, C., Gaul, D., Kolb, A., Schmiedinger, I., Huwe, B., 2010. Investigating flow mechanisms in a forest soil by mixed effects modeling. Eur. J. Soil Sci. 61, 1079–1090.
Bouwer, H., 1986. Intake rate: cyliner infiltrometer. In: Klute, A. (Ed.), Methods of Soil Analysis, Part 1. Physical and Mineralogical Methods. Am. Soc. Agron., Madison, WI, pp. 760–784.
Bundt, M., Widmer, F., Pesaro, M., Zeyer, J., Blaser, P., 2001. Preferential flow paths: biological 'hot spots' in soils. Soil Biol. Biochem. 33, 729–738.
Cerda, A., 1997. Seasonal changes of the infiltration rates in a Mediterranean scrubland on limestone. J. Hydrol. 198, 209–225.
Cey, E.E., Rudolph, D.L., 2009. Field study of macropore flow processes using tension infiltration of a dye tracer in partially saturated soils. Hydrol. Process. 23, 1768–1779.
De Vries, J., Chow, T.L., 1978. Hydrologic behavior of a forested mountain soil in coastal British Columbia. Water Resour. Res. 14, 935–942.
Devitt, D.A., Smith, S.D., 2002. Root channel macropores enhance downward movement of water in a Mojave Desert ecosystem. J. Arid Environ. 50, 99–108.
Flury, M., Wai, N.N., 2003. Dyes as tracers for vadose zone hydrology. Rev. Geophys. 41, 30–31.
Flury, M., Flühler, H., Jury, W.A., Leuenberger, J., 1994. Susceptibility of soils to preferential flow of water: a field study. Water Resour. Res. 30, 1945–1954.
Flury, M., Flühler, H., 1994. Brilliant blue FCF as a dye tracer for solute transport studies a toxicological overview. J. Environ. Qual. 23, 1108–1112.
Germann, P., Helbling, A., Vadilonga, T., 2007. Rivulet approach to rates of preferential infiltration. Vadose Zone J. 6, 207–220.
Germann, P.F., Lange, B., Lüscher, P., 2012. Preferential flow dynamics and plant rooting systems. In: Hydropedology, pp. 121–141.
Ghodrati, M., Jury, W.A., 1990. A field study using dyes to characterize preferential flow of water. Soil Sci. Soc. Am. J. 54, 1558–1563.
Hendrickx, J.M., Flury, M., 2001. Uniform and preferential flow mechanisms in the vadose zone. In: Conceptual Models of Flow and Transport in the Fractured Vadose Zone, pp. 149–187.
Huang, Z., Tian, F.P., Wu, G.L., Liu, Y., Dang, Z.Q., 2017. Legume grasslands promote precipitation infiltration better than gramineous grasslands in arid regions. Land Degrad. Dev. 28, 309–316.
Iserloh, T., Ries, J.B., Arnáez, J., Boix-Fayos, C., Butzen, V., Cerdà, A., Wirtz, S., 2013. European small portable rainfall simulators: a comparison of rainfall characteristics. Catena 110, 100–112.
Jaromir, D., Tomas, V., 2018. Hillslope hydrograph separation: the effects of variable isotopic signatures and hydrodynamic mixing in macroporous soil. J. Hydrol. 563, 446–459.
Jarvis, N.J., Moeys, J., Koestel, J., Hollis, J.M., 2012. Preferential flow in a pedological perspective. In: Hydropedology, pp. 75–120.
Jia, X.X., Shao, M.A., Zhu, Y.J., Luo, Y., 2017. Soil moisture decline due to afforestation across the Loess Plateau, China. J. Hydrol. 546, 113–122.
Jia, X.X., Shao, M.A., Yu, D.X., Zhang, Y., Binley, A., 2019. Spatial variations in soil-water carrying capacity of three typical revegetation species on the Loess Plateau, China. Agric. Ecosyst. Environ. 273, 25–35.
Jiang, X.J., Liu, W., Wu, J., Wang, P., Liu, C., Yuan, Z.Q., 2017. Land degradation controlled and mitigated by rubber–based agroforestry systems through optimizing soil physical conditions and water supply mechanisms: a case study in Xishuangbanna, China. Land Degrad. Dev. 28, 2277–2289.
Jiang, X.J., Liu, W.J., Chen, C.F., Liu, J.Q., Yuan, Z.Q., Jin, B.C., Yu, X.Y., 2018. Effects of three morphometric features of roots on soil water flow behavior in three sites in China. Geoderma 320, 161–171.
Keesstra, S., Pereira, P., Novara, A., Brevik, E.C., Azorin-Molina, C., Parras-Alcántara, L., Cerdà, A., 2016. Effects of soil management techniques on soil water erosion in apricot orchards. Sci. Total Environ. 551–552, 357–366.
Lassu, T., Seeger, M., Peters, P., Keesstra, S.D., 2015. The Wageningen rainfall simulator: Set-up and calibration of an indoor nozzle-type rainfall simulator for soil erosion studies. Land Degrad. Dev. 26, 604–612.
Liu, H., Lei, T.W., Zhao, J., Yuan, C.P., Fan, Y.T., Qu, L.Q., 2010. Effects of rainfall intensity and antecedent soil water content on soil infiltrability under rainfall conditions using the run off-on-out method. J. Hydrol. 396, 24–32.
Logsdon, S.D., Jaynes, D.B., 1993. Methodology for determining hydraulic conductivity with tension infiltrometers. Soil Sci. Soc. Am. J. 57, 1426–1431.
López-Vicente, M., Álvarez, S., 2018. Stability and patterns of topsoil water content in rainfed vineyards, olive groves, and cereal fields under different soil and tillage conditions. Agr. Water Manage. 201, 167–176.
López-Vicente, M., Navas, A., 2009. Predicting soil erosion with RUSLE in Mediterranean agricultural systems at catchment scale. Soil Sci. 174, 272–282.
Ma, B., Liang, X., Liu, S., Jin, M., Nimmo, J.R., Li, J., 2017. Evaluation of diffuse and preferential flow pathways of infiltrated precipitation and irrigation using oxygen and hydrogen isotopes. Hydrogeol. J. 25, 675–688.
Mao, L.L., Lei, T.W., Bralts, V.F., 2011. An analytical approximation method for the linear source soil infiltrability measurement and its application. J. Hydrol. 411, 169–177.
Mao, L.L., Li, Y.Z., Hao, W.P., Mei, X.R., Bralts, V.F., Li, H.R., Guo, R., Lei, T.W., 2016. An approximate point source method for soil infiltration process measurement. Geoderma 264, 10–16.
Meek, B.D., De Tar, W.R., Rolph, D., Rechel, E.R., Carter, L.M., 1990. Infiltration rate as affected by an alfalfa and no-till cotton cropping system. Soil Sci. Soc. Am. J. 54, 505–508.
Mitchell, W.T., 1995. Picture Theory: Essays on Verbal and Visual Representation. University of Chicago Press.
Mitchell, A.R., Ellsworth, T.R., Meek, B.D., 1995. Effect of root systems on preferential flow in swelling soil. Soil Sci. Plant Anal. 26, 2655–2666.
Ogden, C.B., Van Es, H.M., Schindelbeck, R.R., 1997. Miniature rain simulator for measurement of infiltration and runoff. Soil Sci. Soc. Am. J. 61, 1041–1043.
Perroux, K.M., White, I., 1988. Design for disc permeameters. Soil Sci. Soc. Am. J. 52, 1205–1215.
Peterson, A.E., Bubenzer, G.D., 1986. Intake rate: sprinkler infiltrometer. In: Klute, A. (Ed.), Methods of Soil Analysis. Part 1. Physical and Mineralogical Methods. Am. Soc. Agron., Madison, WI, pp. 784–810.
Reynolds, W.D., Elrick, D.E., 1990. Ponded infiltration from a single ring. I. analysis of steady state flow. Soil Sci. Soc. Am. J. 54, 1233–1241.
Reynolds, W.D., Zebchuk, W.D., 1996. Use of contact material in tension infiltrometer measurements. Soil Technol. 9, 141–159.
Rodrigo Comino, J., Sinoga, J.D.R., Senciales González, J.M., Guerra-Merchán, A., Seeger, M., Ries, J.B., 2016. High variability of soil erosion and hydrological processes in Mediterranean hillslope vineyards (Montes de Málaga, Spain). Catena 145, 274–284.
Rodrigo Comino, J., Bogunovic, I., Mohajerani, H., Pereira, P., Cerdà, A., Sinoga, J.D.R., Ries, J.B., 2017. The impact of vineyard abandonment on soil properties and hydrological processes. Vadose Zone J. 16, 1–7.
Smets, T., López-Vicente, M., Poesen, J., 2011. Impact of subsurface rock fragments on runoff and interrill soil loss from cultivated soils. Earth Surf. Process. Landf. 36, 1929–1937.
Su, N.H., 2007. Radial water infiltration-advance-evaporation processes during irrigation

using point source emitters in rigid and swelling soils. J. Hydrol. 344, 190–197.
Walsh, E., McDonnell, K.P., 2012. The influence of measurement methodology on soil infiltration rate. Int. J. Soil Sci. 7, 168–176.
Wang, X.P., Li, X.R., Xiao, H.L., Berndtsson, R., Pan, Y.X., 2007. Effects of surface characteristics on infiltration patterns in an arid shrub desert. Hydrol. Process. 21, 72–79.
Wang, X.P., Cui, Y., Pan, Y.X., Li, X.R., Yu, Z., Young, M.H., 2008. Effects of rainfall characteristics on infiltration and redistribution patterns in revegetation-stabilized desert ecosystems. J. Hydrol. 358, 134–143.
Wang, R.Y., Strong, D.M., 1996. Beyond accuracy: what data quality means to data consumers. J. Manage. Inf. Syst. 12, 5–33.
Weiler, M., 2005. An infiltration model based on flow variability in macropores: development, sensitivity analysis and applications. J. Hydrol. 310, 294–315.
Weiler, M., Flühler, H., 2004. Inferring flow types from dye patterns in microporous soils. Geoderma 120, 137–153.
Weiler, M., Naef, F., 2003. An experimental tracer study of the role of macropores in infiltration in grassland soils. Hydrol. Process. 17, 477–493.
Wu, G.L., Liu, Y., Yang, Z., Cui, Z., Deng, L., Chang, X.F., Shi, Z.H., 2017. Root channels to indicate the increase in soil matrix water infiltration capacity of arid reclaimed mine soils. J. Hydrol. 546, 133–139.
Wu, L., Pan, L., Roberson, M.J., Shouse, P.J., 1997. Numerical evaluation of ring-infiltrometers under various soil conditions. Soil Sci. 162, 771–777.
Wu, L., Pan, L., Mitchel, J., Sanden, B., 1999. Measuring saturated hydraulic conductivity using generalized solution for single-ring infiltrometers. Soil Sci. Soc. Am. J. 63, 788–792.
Wu, G.L., Yang, Z., Cui, Z., Liu, Y., Fang, N.F., Shi, Z.H., 2016. Mixed artificial grasslands with more roots improved mine soil infiltration capacity. J. Hydrol. 535, 54–60.
Yin, M.H., Li, Y.N., Xu, Y.B., Zhou, C.M., 2018. Effects of mulches on water use in a winter wheat/summer maize rotation system in Loess Plateau, China. J. Arid Land 10, 277–291.
Zhang, J., Lei, T.W., Chen, T.Q., 2016. Impact of preferential and lateral flows of water on single-ring measured infiltration process and its analysis. Soil Sci. Soc. Am. J. 80, 859–869.
Zhang, Y.H., Niu, J.Z., Yu, X.X., Zhu, W.L., Du, X.Q., 2015. Effects of fine root length density and root biomass on soil preferential flow in forest ecosystems. Forest Syst. 24, 012.
Zhang, Y., Niu, J., Zhang, M., Xiao, Z., Zhu, W., 2017. Interaction between plant roots and soil water flow in response to preferential flow paths in Northern China. Land Degrad. Dev. 28, 648–663.